Direct Imaging of Anisotropic Exciton Diffusion and Triplet Diffusion Length in Rubrene Single Crystals

Pavel Irkhin and Ivan Biaggio

Department of Physics, Lehigh University, Bethlehem, Pennsylvania 18015, USA

(Received 9 February 2011; published 1 July 2011)

We visualize exciton diffusion in rubrene single crystals using localized photoexcitation and spatially resolved detection of excitonic luminescence. We show that the exciton mobility in this material is strongly anisotropic with long-range diffusion by several micrometers associated only with the direction of molecular stacking in the crystal, along the *b* axis. We determine a triplet exciton diffusion length of 4.0 ± 0.4 μm from the spatial exponential decay of the photoluminescence that originates from singlet excitons formed by triplet-triplet fusion.

DOI: 10.1103/PhysRevLett.107.017402 PACS numbers: 78.55.Kz, 71.35.−y, 81.05.Fb, 88.40.jr

Organic molecular crystals operate in an unusual, relatively unexplored region in the landscape of solid-state physics. It is a region characterized by narrow energy bands with transport at the boundary between hopping and coherent band-transport, and where photon absorption results in tightly bound excitons that limit free-carrier generation. Fundamental studies of exciton dynamics in organic crystals are important for understanding the role of intermolecular interactions in exciton transport, and are of prime interest towards the optimization of photocarrier generation in organic photovoltaics, where exciton diffusion is a key process limiting the photovoltaic efficiency [1,2]. However, direct experimental observations of exciton diffusion have proven difficult, and most available data were obtained by indirect methods [3–5], resulting in a relatively large variability between the reported diffusion lengths for the same materials [6,7].

The experimental investigation of exciton diffusion is a challenging task, especially in disordered molecular materials, where the exciton diffusion length is very short, of the order of a few tens of nanometers [2,8,9]. Organic molecular crystals with their intrinsic order, on the other hand, should allow for longer-range diffusion, and are also attractive for fundamental investigations. In fact, initial estimates put diffusion lengths in molecular crystals in the range of a few micrometers [10]. Early work done in anthracene, mostly using indirect methods, claimed diffusion lengths of up to 10 μm [3–5]. Literature on other crystals such as tetracene or rubrene is more limited [6,7,11]. In particular, the rubrene crystal has several compelling properties, including one of the highest room-temperature charge carrier mobilities ever observed in an organic material ($\sim$ 10–40 $\mathrm{cm^2\,V^{-1}\,s^{-1}}$ for holes in field-effect transistors [12,13]) and a high photoconductivity [14]. In addition, recent photoconductivity studies in rubrene [11] have been interpreted in terms of long exciton diffusion lengths of several micrometers that would allow excitons to migrate to the crystal surface, but no direct observations of exciton diffusion have been reported yet. Motivated by the importance of exciton migration for the photoconductivity process and by the interest of rubrene as a material for optoelectronics, we now developed a direct imaging technique to observe exciton diffusion.

Rubrene crystals grown by physical vapor transport have an orthorhombic unit cell with lattice parameters $a = 14.4$ Å, $b = 7.18$ Å, and $c = 26.9$ Å [15]. Our definition of crystallographic axes corresponds to that used in several charge transport experiments [12], and goes over to that used in Ref. [16] by switching the *a* and *b* axes, and to that used in Ref. [15] by switching the *a* and *c* axes. The most common crystal shapes are platelets with extended *c*-surfaces and crystals elongated in the *b* direction but with short dimensions in the *a* and *c* directions. As-grown rubrene crystals have facets that form a typical angle of 63.5° (75°) to the *b* axis when observing the *ab* (*bc*) plane (see Fig. 1).

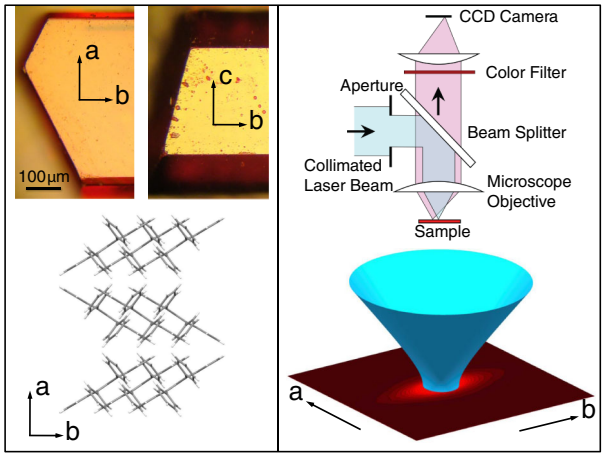

FIG. 1 (color online). Top-left: *ab* and *bc* facets of rubrene single crystals. Bottom-left: molecular packing in the crystal and definition of crystallographic axes. Top-right: experimental configuration. Bottom-right: scheme of the illumination conditions at the surface of the crystal.

We visualize the presence of excitons and their diffusion by imaging the photoluminescence (PL) that originates from their radiative recombination after localized photoexcitation at well defined crystal surfaces. This straightforward method provides direct, intuitive images of the spatial exciton distribution. Its principles have been previously applied in inorganic semiconductors [17], but only under challenging cryogenic conditions required by the low binding energy of excitons. Thanks to the large excitonic binding energies in molecular crystals, we have now succeeded in creating the experimental conditions that allow direct imaging of exciton diffusion at room-temperature.

The experimental setup is described in Fig. 1. We create a localized distribution of excitons via a collimated continuous wave laser beam with a wavelength in the high absorption region of rubrene (442 nm, absorption length of $\sim 2\ \mu$m) that is focused on the sample by a microscope objective. The same microscope objective images the surface of the sample onto a CCD camera. By changing color filters, we can photograph the surface of the sample using either the excitation light, or the PL coming from excitons (with a filter transmitting above 500 nm). We use a well-corrected, variable numerical aperture infinite conjugate microscope objective to obtain the optimum combination of illumination profile, depth of field ($\sim 2\ \mu$m), and lateral resolution ($\sim 0.5\ \mu$m). A small amount of truncation results in the excitation light intensity being a hybrid between an Airy pattern and a Gaussian distribution. The spot size is 1.1 μm, defined as the diameter at which the intensity falls to $1/e^2$ of its peak value. Figure 1 (bottom-right) is a schematic view of the excitation beam focused on the sample surface and the PL it generates.

Figure 2 shows the intensity distribution of the excitation light and of the PL as we typically observed them at the surface of all rubrene samples we studied. Independently of the shape, size, orientation,or thickness of a crystal, as long as we illuminate a surface that contains the b axis, we observe a pattern like that in Fig. 2. While the excitation is perfectly round and symmetric, the PL is clearly elongated along the b axis of the crystal, corresponding to a highly anisotropic exciton diffusion. We obtained the same results for both the ab facet and the bc facet of several rubrene crystals. The depth of field of the imaging system is of the order of the absorption length of the excitation light. This, combined with our observation of no relevant diffusion in the direction perpendicular to the surface of the crystal, guarantees that the whole distribution of diffusing excitons is sharply imaged. The significantly higher exciton mobility in the b direction correlates well with the high charge carrier mobility observed in the same direction [12,13].

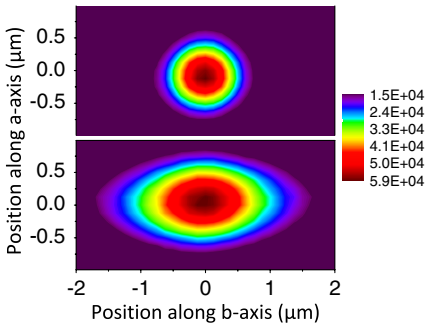

FIG. 2 (color online). Contour plot of the intensity distribution of the excitation light (top) and of the PL at the surface of a rubrene sample (bottom).

For the b direction, it was possible to follow the decay of the PL intensity over 3 orders of magnitude for increasing distances from the center of the illumination. Figure 3 shows the spatial dependence along the b axis for both excitation profile and PL profile taken in five samples grown at different times and under different conditions that created crystal shapes ranging from flat platelets and elongated needles to submillimeter sized microcrystals. The excitation and emission profiles are normalized to the same level at the center of the illumination. The excitation light decays very rapidly as highlighted by the semilogarithmic scale in the plot, but the PL extends over much larger distances. The reproducibility of the data from all five samples shown in the figure is very good, and the spatial dependence at larger distances from the center can be fitted for all samples simultaneously by an exponential function $\exp(-x/d)$, where x is the distance from the center of the excitation spot and $d = 2.0 \pm 0.2\ \mu$m.

The data in Fig. 3 were taken at a laser power of 10 nW, which still gives a good signal-to-noise ratio while avoiding overexposure of the crystal. This power corresponds to a flux of $\sim$20 photons per nanosecond incident on the 1.1 μm diameter spot and absorbed with an exponential absorption length of 2.0 μm. This gives an absorbed photon rate of ~ 10 photons $\mathrm{ns}^{-1}\ \mu\mathrm{m}^{-3}$. Photon absorption

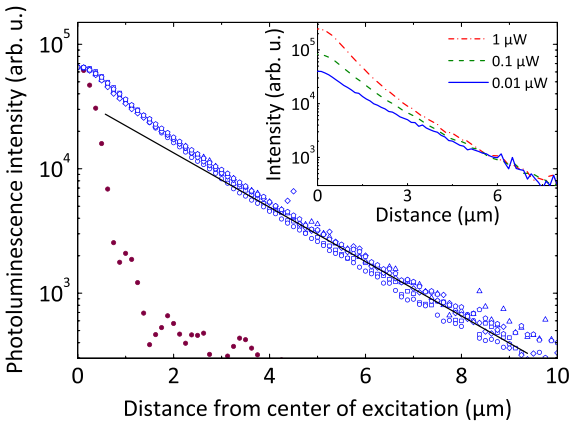

FIG. 3 (color online). Intensity of the excitation light (full red symbols) and intensity of the PL emitted by the diffusing excitons (open blue symbols) vs the distance from the center of the excitation spot along the b axis of the crystal. The PL data belong to five different crystals, represented by different symbols for the data points. Inset: Normalized PL profiles obtained at different laser powers.

results in a singlet molecular exciton with a lifetime of less than 10 ns [14], meaning that at any given time there are less than 100 μm^{-3} singlets in the excitation spot. This corresponds to a singlet exciton for every 10 million rubrene molecules, and shows that our exposure conditions remain a relatively small perturbation.

We now turn to the discussion of how the PL data should be interpreted. Measurements of the PL time dynamics in rubrene have shown that an initial fast decay that happens in less than 10 ns is followed by a relatively strong PL that decays much more slowly [14]. This indicates that directly photoexcited singlet excitons have a lifetime of less than 10 ns and that many of them undergo fission [18,19] to create longer lived triplet excitons. The PL seen at later times is then the result of triplets interacting with each other and fusing, pooling their energy to create again a singlet exciton, which subsequently radiatively decays [19]. Even though the PL is always caused by the radiative decay of zero-momentum singlets, this effect makes it possible for our experiment to detect the density of triplet excitons. Because of the large diffusion anisotropy, we can describe the spatial dependence of the triplet density T with the following one-dimensional diffusion equation:

$$\frac{d}{dt}T = G + D\frac{d^2}{dx^2}T - \frac{T}{\tau_T} - \gamma T^2, \qquad (1)$$

where x is the coordinate along the b direction, G represents the source function for the creation of excitons (directly given by our excitation profile), D is the diffusion constant along the b axis, and the last two terms on the right-hand side take into account the triplet lifetime τ_T (dominant at low triplet densities) and triplet-triplet collisions (dominant at high densities). The solution of the above diffusion equation in steady state and at the low triplet densities found far away from the excitation region—where the last term on the right-hand has a negligible influence on the triplet exciton density—is $T(x) = T_0 \exp(-x/L_D)$, with the diffusion length $L_D = \sqrt{\tau_T D}$, the typical solution valid for any diffusion process of particles with a limited lifetime.

The spatially exponential PL decay in Fig. 3 can thus be assigned to an exponentially decaying density of triplet excitons, at densities where triplet-triplet interaction still provides for the PL by producing singlet excitons, but where the term T/τ_T is dominant in Eq. (1) [19]. Under these conditions the PL intensity, given by the rate of decay of singlet excitons, is proportional to the rate at which singlet excitons are formed from triplets, and is therefore proportional to the square of the triplet density [19]. This means that the spatial exponential decay in Fig. 3, with a decay constant of 2.0 ± 0.2 μm, corresponds to a triplet exciton diffusion length $L_D = 4.0 \pm 0.4$ μm. We note that we observe the same PL pattern and the same diffusion length in several rubrene crystals, including samples that have been artificially exposed to oxygen. We have confirmed that the crystal's surface has no effect on the observed diffusion by varying the excitation wavelength between 442 nm and 532 nm and showing that the corresponding change in the depth of exciton generation does not influence the PL pattern. In addition, we have also seen the same PL pattern when the sample surface was coated with fomblin oil. The observed long-range diffusion must be an intrinsic property of rubrene.

The interpretation of the long-range diffusion as triplet diffusion is also supported by our observation that an increase in illumination power, and thus of exciton density, leads to a PL intensity that is disproportionally higher close to the center of the excitation spot, and to a transition to a pure exponential decay that happens at larger distances (Fig. 3, inset). Such behavior is consistent with the nonexponential spatial decay of the triplet density that is predicted by Eq. (1) at higher densities. There could also be a contribution of PL emitted directly by photoexcited singlet excitons, but further experiments will be needed to determine the role of singlet exciton diffusion, if any.

The large diffusion length that we observe along the b axis is likely related to the molecular arrangement that forms stacks of molecules in the b direction [15,16], and that is also responsible for the exceptionally high hole mobility observed in the same direction. The large exciton diffusion seen in Fig. 2 is indeed a peculiarity of rubrene. As an example, we performed preliminary imaging experiments in tetracene but we could not detect any such spread of the PL, hinting at a short diffusion length, in agreement with Ref. [6] but casting some doubts on other early measurements of long diffusion lengths [7]. Our results are also important in view of recent photoconductivity experiments that were interpreted as a sign of long-range diffusion in the c direction [11]. While Ref. [11] hypothesizes an exciton diffusion length of the order of 5 μm in the c direction, at such a distance in the c direction we cannot detect any excitonic PL. Our direct imaging results leave little doubt that only in the b direction can a large amount of photoinduced excitons migrate by a few micrometers. Further studies will now be necessary that integrate our direct imaging technique with photoconductivity experiments such as those presented in Ref. [11]. In any case, the strong exciton diffusion anisotropy that we have seen will play an important role in the design of future photoconductivity or photovoltaic experiments in rubrene.

We conclude this report with two examples that further illustrates the flexibility of the exciton imaging technique that we presented. In Fig. 4 we show the intensity distribution of the PL obtained in a sample consisting of a ~ 1 μm thin rubrene crystal that spontaneously grew on the bc facet of a larger rubrene crystal, but with its b axis at an angle of $\sim 100°$ to the b axis of the larger crystal below it. Performing the exciton diffusion experiment at point A (see Fig. 4) creates excitons both inside the small thin crystal as well as inside the large crystal below it. Independent diffusion of the two exciton populations leads to a PL distribution that is clearly a superposition of two independent ovals, one belonging to the excitons that

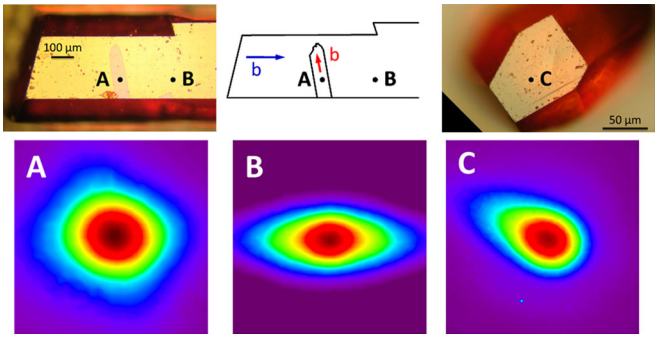

FIG. 4 (color online). Top: crystal facets and locations where exciton diffusion experiments were performed. (A) Micrometer thin crystal that grew on top of a *bc* facet, but has a different orientation. The PL pattern shows the effect of exciton diffusion occurring at the same time in the thin crystal and in the crystal below it. (B) Clean *bc* facet. Normal anisotropic exciton diffusion. (C) A crystal facet where the *b* axis is not parallel to the surface, which produces an asymmetric PL pattern oriented along the projection of the *b* axis on the surface. All contour plots cover an area of $5 \times 5\ \mu m^2$.

diffuse inside the small crystal, and one belonging to the excitons inside the larger crystal. The elongations in the PL pattern are at an angle of $\sim 100°$ to each other, matching the orientation of the two *b* axes in the two crystals. In addition, we obtained PL patterns from several facets of rubrene microcrystals [20] where the *b* axis was not parallel to the surface and Fig. 4 shows an example of what happens in this case. The asymmetry of the pattern obtained in point *C* of is caused by excitons that diffuse along the *b* axis, but immediately reach the surface in one direction while they go deeper into the crystal in the other direction. As these examples demonstrate, an important and attractive characteristic of the imaging technique that we have demonstrated in this work is its directness. It is flexible, it can be readily used under different experimental conditions, and it allows us to establish the presence of exciton diffusion as long as the diffusion length is at least larger than the optical resolution of the imaging system, or in other words of the order of 1 μm.

In conclusion, we used a direct imaging technique to observe exciton diffusion and exciton mobility anisotropy in molecular crystals, and we have determined a triplet diffusion length of $4.0 \pm 0.4\ \mu$m along the *b* axis of rubrene single crystals. The imaging technique we have demonstrated will enable the investigation of exciton diffusion under different experimental conditions and in different materials, opening the doors to extensive new investigations of exciton diffusion phenomena, and ultimately providing important new knowledge on exciton transport processes in organic molecular crystals.

We thank V. Podzorov at Rutgers University for providing the rubrene samples. We acknowledge support from a Faculty Innovation Grant from Lehigh University.

[1] G. Yu, J. Gao, J. C. Hummelen, F. Wudl, and A. J. Heeger, Science **270**, 1789 (1995).
[2] P. Peumans, S. Uchida, and S. R. Forrest, Nature (London) **425**, 158 (2003).
[3] P. Avakian and R. E. Merrield, Phys. Rev. Lett. **13**, 541 (1964).
[4] V. Ern, P. Avakian, and R. E. Merrield, Phys. Rev. **148**, 862 (1966).
[5] D. F. Williams and J. Adolph, J. Chem. Phys. **46**, 4252 (1967).
[6] G. Vaubel and H. Kallmann, Phys. Status Solidi B **35**, 789 (1969).
[7] W. Arden, M. Kotant, and L. M. Peter, Phys. Status Solidi B **75**, 621 (1976).
[8] Y. Terao, H. Sasabe, and C. Adachi, Appl. Phys. Lett. **90**, 103515 (2007).
[9] H. Gommans, S. Schols, A. Kadashchuk, P. Heremans, and S. C. J. Meskers, J. Chem. Phys. C **113**, 2974 (2009).
[10] J. Jortner, S.-i. Choi, J. L. Katz, and S. A. Rice, Phys. Rev. Lett. **11**, 323 (1963).
[11] H. Najafov, B. Lee, Q. Zhou, L. C. Feldman, and V. Podzorov, Nature Mater. **9**, 938 (2010).
[12] V. Podzorov, V. Pudalov, and M. Gershenson, Appl. Phys. Lett. **82**, 1739 (2003); V. Podzorov, E. Menard, A. Borissov, V. Kiryukhin, J. A. Rogers, and M. E. Gershenson, Phys. Rev. Lett. **93**, 086602 (2004); V. Podzorov and M. Gershenson, *ibid.***95**, 016602 (2005); V. C. Sundar, J. Zaumseil, V. Podzorov, E. Menard, R. L. Willett, T. Someya, M. E. Gershenson, and J. A. Rogers, Science **303**, 1644 (2004).
[13] T. Hasegawa and J. Takeya, Sci. Tech. Adv. Mater. **10**, 024314 (2009).
[14] H. Najafov, I. Biaggio, V. Podzorov, M. F. Calhoun, and M. E. Gershenson, Phys. Rev. Lett. **96**, 056604 (2006); H. Najafov, B. Lyu, I. Biaggio, and V. Podzorov, Phys. Rev. B **77**, 125202 (2008).
[15] O. D. Jurchescu, A. Meetsma, and T. T. M. Palstra, Acta Crystallogr. Sect. B **62**, 330 (2006).
[16] D. A. Da Silva Filho, E.-G. Kim, and J.-L. Bredas, Adv. Mater. **17**, 1072 (2005).
[17] D. Sanvitto, F. Pulizzi, A. J. Shields, P. C. M. Christianen, S. N. Holmes, M. Y. Simmons, D. A. Ritchie, J. C. Maan, and M. Pepper, Science **294**, 837 (2001).
[18] V. V. Tarasov, G. E. Zoriniants, A. I. Shushin, and M. M. Triebel, Chem. Phys. Lett. **267**, 58 (1997).
[19] M. Pope and C. Swenberg, *Electronic Processes in Organic Crystals and Polymers* (Oxford University Press, Oxford, NY, 1999).
[20] M. El Helou, O. Medenbach, and G. Witte, Cryst. Growth Des. **10**, 3496 (2010).